The origin of pyroelectricity in boracite at varying temperatures

Qiang-qiang wang
China University of Geosciences
ruijin sun (srj@cugb.edu.cn)
China University of Geosciences
Jie-Sen Guo
Beihang University
Yue-Tong Wu
China University of Geosciences
Yu-Xin Ma
China University of Geosciences
Fei Chen
China University of Geosciences
Tian-Ming Liu
China University of Geosciences
Hao-Dong Li
China University of Geosciences
Fan-Shu Meng
China University of Geosciences
De-Zhong Meng
China University of Geosciences
Chang-Chun Zhao
China University of Geosciences

Research Article

Keywords:

Posted Date: January 5th, 2023

DOI: https://doi.org/10.21203/rs.3.rs-2437032/v1

Abstract

Chambersite ($Mn_3B_7O_{13}Cl$) has excellent pyroelectric performance and promised to be a low-cost substitute for $LiTaO_3$ and a non-toxic alternative to $PbTiO_3$ in many application scenarios. However, the origin and mechanism of pyroelectricity in $Mn_3B_7O_{13}Cl$ at varying temperatures remain to be studied. In this work, we report the temperature-dependent crystal structure information via X-ray diffraction refinement, and based on this, we calculated the intrinsic electric dipole moments of the typical coordination polyhedral ([$ClMn_6$]) in $Mn_3B_7O_{13}Cl$ unit cell along the c-axis at various temperature ranging from 300 to 400 K. The calculated pyroelectric coefficients based on the intrinsic electric dipole moments were in line with the experimental results, based on the above results, we can conclude that the origin of pyroelectricity in $Mn_3B_7O_{13}Cl$ is mainly the distortion of the $ClMn_6$ polyhedron along the c-axis. Our work has understood the pyroelectric mechanism of $Mn_3B_7O_{13}Cl$, and has played a positive role in promoting the modifications and applications for $Mn_3B_7O_{13}Cl$ and other boracite minerals.

1. Introduction

Chambersite ($Mn_3B_7O_{13}Cl$) is a rare mineral with a polar point group(mm2)(Honea et al. 1962; Kubel and Crottaz et al. 1996). The novel properties of $Mn_3B_7O_{13}Cl$ have boosted fundamental studies and technological advancements for a wide range of applications. The $Mn_3B_7O_{13}Cl$ consists of a nonvanishing dipole moment, wherein the piezo-/pyro-/ferroelectric properties existed(Castellanos-guzman et al. 1981; Castellanos-Guzman et al. 1994; Crottaz et al. 1998). In recent years, high-crystallized $Mn_3B_7O_{13}Cl$ could improve the deep-ultraviolet coherent light production with quasi-phase-matching(Xiong et al. 2020; Wang et al. 2018; Xiong et al. 2016). Former works investigated the magnetic behavior of $Mn_3B_7O_{13}Cl$. Neutron deflection and symmetry analysis confirmed the antiferromagnetic sequence of TN about 10K(Schnelle and Schmid et al. 2015). In addition, nanorods-type $Mn_3B_7O_{13}Cl$ was used in the fields of anti-wear properties of base oils and anodes for lithium-ion batteries(Aihua et al. 2015).

Among all the applications, the pyroelectric performance of $Mn_3B_7O_{13}Cl$ was particularly concerning(Schmid et al. 1980; Campa-Molina et al. 1994; Bhalla et al. 1985). The pyroelectricity effect is a kind of functional characteristic that attracts wide attention and has been widely applied in infrared radiation, temperature detector, waste heat harvesters et al(Kuznetsov et al. 2016; Lheritier et al. 2022; Zhang et al. 2021; Pandya et al. 2019; Shirokov et al. 2017). The previous literature shows the excellent pyroelectric performance of $Mn_3B_7O_{13}Cl$ which are promised to be a low-cost substitute for $LiTaO_3$ and a non-toxic alternative to $PbTiO_3$ in many application scenarios.(Jayalakshmy et al. 2014; Liang et al. 2015; Bhatti et al. 2016; Xu et al. 2013). Pyroelectricity relies on the temperature-dependent variety of electric dipole moments(Yang et al. 1994; Lang et al. 2005). When the temperature is less than 690K, $Mn_3B_7O_{13}Cl$ undergoes a structural phase transition from the cubic to the orthorhombic crystal system, and crystallize at room temperature with the spatial point group of $Pca2_1$. The Cl ion of ClMn6 octahedron deviates from

the center of the octahedron, resulting in structural distortion, spontaneous polarization and electric dipole moment(Guo et al. 2022). However, so far, we still haven't figured out the detailed relationship between the distortion of ClMn6 polyhedron and spontaneous polarization in $Mn_3B_7O_{13}Cl$, hence the origin of pyroelectricity is still to be studied.

Herein, we report the temperature-dependent structures and pyroelectric coefficients for $Mn_3B_7O_{13}Cl$. The calculations of distortion parameters of the ClMn6 polyhedron suggest that the intrinsic electric dipole comes from the distortion of the ClMn6 polyhedron along the c-axis. Further calculations of pyroelectric coefficients using the temperature-dependent distortion parameters of the ClMn6 polyhedron are in line with experimental data. Our results illustrate the mechanism for spontaneous polarization and pyroelectric in $Mn_3B_7O_{13}Cl$, which is of great value for improving the pyroelectric performance of $Mn_3B_7O_{13}Cl$ and other isostructural materials.

2. Experimental

2.1. Polycrystalline $Mn_3B_7O_{13}Cl$ and $Ni_3B_7O_{13}Cl$ synthesis

$Mn_3B_7O_{13}Cl$ was synthesized by solution synthesis method (Delfino et al. 1980; Wang et al. 2013). Firstly, the stoichiometric ratio of $Mn_3B_7O_{13}Cl$ was referred to for formulation. Using 0.6mol $MnCl_2{\cdot}4H_2O$ and 0.35mol $Na_2B_4O_7{\cdot}10H_2O$ as initial raw materials, the solution was dissolved in a beaker with water, and ammonia was added to make the solution neutral. After drying in the oven, the drying sample is put into the Muffle furnace for calcination, after washing, filtering, drying, grinding to obtain high purity cubic borite powder crystal sample. The drying temperature was selected as 363K and the roasting temperature as 833K. Ni3B7O13Cl was synthesized by the same method.

2.2. Characterization and property test

The phase of synthesis samples was characterized by X-ray diffpraction(XRD) on Panalytical In this paper, A PANalytical XRD diffraction instrument has been used to analyze the phase of the sample. The target material used in the test is Cu K target, the wavelength of the target is 1.54056 A, the range of 2θ scanning is 10°-80°, and the scanning rate is 2 °/min.

The XRD data of powder structure finishing were scanned by step-size scanning, the step speed was 0.01° per step, the residence time of each step was 1 s, the 2θ scanning range was 10°-130°, the operating voltage was 40 KV, the operating current was 40 mA.

The scanning electron microscope (SEM) JSM-6510A/JSM-6510LA and EDS were integrated to complete the whole process from image observation to element analysis.

The pyroelectric testing instrument is TF analyzer 3000 ferroelectric comprehensive tester produced by aix ACCT Company in Germany. The test temperature range chosen in this study is 300 ~ 400K, and the heating rate is 5k/min. TF-3000 Keysight E49990A pulse analysis system was used to measure the

dielectric coefficient and dielectric loss. The test condition was selected as room temperature, and the frequency was changed manually to obtain the test parameters at different frequencies.

The instrument used in the infrared spectroscopy test is the American Thermo Fisher Fourier transform infrared spectrometer Nicolet 6700FTIR (Experimental conditions: wave-number scanning range of 400–2000 cm-1, resolution of 0.35 cm-1, the test temperature is 25℃).

3. Results And Discussions

3.1 Crtstal structure of $Mn_3B_7O_{13}Cl$

The crystal structure of Mn3B7O12Cl is shown in Fig. 1 (a), which has a unidirectional polar axis along the C direction and consists of four three-dimensional borate skeletons and four ClMn6 octahedrons sharing manganese atomic links(Nelmes et al. 1974). The structure undergoes a nonpolar to polar structural phase transition at temperatures below 698K, with all Cl ions off-center along the polar axis(McQuaid et al. 2017), which is the source of $Mn_3B_7O_{13}Cl$ spontaneous planning, similar to the typical perovskite material BaTiO3, where Ti ions off-center from the center of the oxygen octahedron. (Guo;Sun;Chen;Hao;Ma;Wang;Wu;Hou;Zhang;Liu;Li;Meng and Zhao et al. 2022; Wang;Qiao;Su;Hu;Yang;He and Long et al. 2018; Sun et al. 2017).

3.2. Characterization of $Mn_3B_7O_{13}Cl$

In order to study the crystal structure change process of $Mn_3B_7O_{13}Cl$ quadborite at different temperatures, XRD test was conducted in situ, and three temperature points were selected at 300K, 350K and 400K. On the basis of in-situ XRD test, in order to obtain more detailed crystal structure information, this study carried out Rietveld refinement on the XRD data obtained to obtain atomic position, cell parameters and other structural information, as shown in tableS1. Figure 1(b) is the comparison between the calculated spectrum and the experimental spectrum after fullprof finishing. The main diffraction peaks of $Mn_3B_7O_{13}Cl$ are well matched with PDF#14–0638(Kubel and Crottaz et al. 1996; Ju et al. 2002), which indicates that the crystal phases of $Mn_3B_7O_{13}Cl$ remain intact at different temperatures. Structural parameters including atomic coordinates, scale factor and unit-cell parameters, can be obtained from at different temperatures(Sri Gyan et al. 2020; Khatun et al. 2022).

Figure 1(c) demonstrate the SEM images of the $Mn_3B_7O_{13}Cl$, and the agglomeration of sample is observed. Moreover, the EDS spectrum in Fig. 1(d) prove that the presence of Mn, B, O and Cl elements in the sample, which are nearly consistent with the chemical constituents.

3.3. Pyroelectric coefficient polyhedron distortion parameters and intrinsic electric dipole moment at varying temperature

3.3.1. The pyroelectric measurements at varying temperature

Pyroelectricity is strictly defined as the temperature dependence of spontaneous polarization in certain anisotropic solids. According to the definition, changes in the intensity of spontaneous polarization are related to changes in temperature as follows (Zhou et al. 2018; Chen et al. 2019; Jachalke et al. 2017)

$$P_s = \frac{d\overrightarrow{D}}{dT} = \frac{d\overrightarrow{P}}{dT}$$

1

which P_s is the pyroelectric coefficient, $\overrightarrow{D}$ is the dielectric displacement, $\overrightarrow{P}$ is the spontaneous polarization, *T* is Kelvin temperature.

As can be seen from Fig. 2, when the sample temperature rises from 300K to 370K, the polarization intensity increases linearly with the increase of temperature, and the average pyroelectric coefficient is 4.5μC/m^2/K in the temperature range of 300-370K, and the pyroelectric coefficient changes little with temperature.

3.3.2. Comparison of calculated and experimental pyroelectric Coefficients

In pyroelectric crystals, electric dipoles usually form with the center of positive charge far away from the center of negative charge. In this study, the electric dipole of $Mn_3B_7O_{13}Cl$ mainly comes from the deformation of ClMn6 octahedron resulting in the non-coincidence of positive and negative electric centers(Wang;Qiao;Su;Hu;Yang;He and Long et al. 2018; Guo;Sun;Chen;Hao;Ma;Wang;Wu;Hou;Zhang;Liu;Li;Meng and Zhao et al. 2022). When the temperature changes, the electric dipole will stretch, resulting in an induced charge on the crystal surface, resulting in a pyroelectric effect, as shown in the Fig. 3(a). In addition, $Mn_3B_7O_{13}Cl$ has a unique axis of rotational symmetry along the C-axis, and polarity occurs at both ends of the *c*-axis. Therefore, only the contribution of the electric dipole moment in the *c* direction to the total electric dipole moment of the cell is considered. The calculation of electric dipole moment is by Formula (2).

$$p = ql$$

2

where q is the charge capacity, l (=△z) is the distance between positive and negative charge center. It can be concluded that the calculation formula of the electric dipole moment in ClMn6 is Formula (3).

$$\sum p == [4 \times 1 \times (\triangle\ Z_X)] \times 1.60 \times 10^{-19}$$

3

$\sum$P is the total electric dipole moment in $ClMn_6$ octahedron, $\triangle$z is the distance between positive and negative charge centers, which is caculated from the atomic positions at different temperatures by Table S1. The intrinsic electric dipole moment of $ClMn_6$ polyhedron in unit cell along the c direction is obtained by using the Formula (3), as shown in Table S2.

According to the relation between pyroelectric coefficient and electric dipole moment, when the crystal volume is constant, the pyroelectric coefficient is proportional to the rate of change of electric dipole moment with temperature.

The intrinsic electric dipole moment fits the equation.

$$P_T = \frac{dp_z}{VdT}$$

4

Where P_T is the pyroelectric coefficient, dp_z is the variable of the intrinsic electric dipole moment at different temperatures, dT is the variable of the temperature during the test, and V is the unit volume.

According to the formula, the pyroelectric coefficients of $Mn_3B_7O_{13}Cl$ in different temperature ranges (300K-350K, 350K-400K) were calculated in this paper, as shown in Fig. 3(b). When the temperature increases, the pyroelectric coefficients in the two temperature ranges increase slightly.

In order to compare the experimentally measured pyroelectric coefficient with the calculated pyroelectric coefficient, we averaged the experimental data for each temperature range, as shown in Fig. 3(b). As can be seen from the figure, the experimental observed value is slightly greater than the theoretical calculated value, so it is inferred that the main structural unit of $Mn_3B_7O_{13}Cl$ pyroelectricity in $ClMn_6$ octahedron.

3.3.3. Calculation of $Mn_3B_7O_{13}Cl$ polyhedron distortion parameters at different temperatures

The pyroelectric properties of materials can be derived from the generation of spontaneous polarization, which is fundamentally due to the symmetry breaking and polyhedral distortion in the crystal structure(Meirzadeh et al. 2019; Chang et al. 2009). Polyhedra in crystal structures are often obtained by distortion of ideal polyhedra(Ertl et al. 2002; Song and Liu et al. 2019; Zhang et al. 1993). A common way to calculate the distortion of a polyhedron is to count the difference between all bond lengths:

$$D = \frac{1}{n}\sum_{i=1}^{n}[(d_i - d_m) / d_m]^2$$

5

Which d_i is polyhedral bond length; d_m average is bond length.

The distortion parameters of $ClMn_6$ polyhedron at different temperatures are calculated. Figure 3(c) shows $Mn_3B_7O_{13}Cl$ boracite polyhedron linearly decrease with the increase of temperature, which indicates that the temperature change will directly cause the deformation of the inner polyhedron, and the degree of deformation of the polyhedron is linear.

3.4. Effect of M - position substitution on pyroelectric coefficient of boracite

Measurement of dielectric and pyroelectric coefficients of $Mn_3B_7O_{13}Cl$ and $Ni_3B_7O_{13}Cl$ In order to investigate the change of pyroelectric property caused by different metal elements occupying M site, nickel boracite powder crystal and manganese boracite powder crystal with similar crystal structure were selected to test the pyroelectric property and dielectric constant. As shown in the Fig. 4, the test results of the two kinds of boracite show that the dielectric coefficient and pyroelectric coefficient of $Mn_3B_7O_{13}Cl$ boracite are larger than those of $Ni_3B_7O_{13}Cl$ boracite, indicating that the polarization and pyroelectric coefficient of the two have a positive correlation law. $Ni_3B_7O_{13}Cl$ has a smaller dielectric coefficient, which may lead to better voltage response and current response values.

Conclusion

In this study, high purity single-phase powder borates ($Mn_3B_7O_{13}Cl$, $Ni_3B_7O_{13}Cl$) were successfully synthesized by a two-step synthesis process combining solution method and solid phase synthesis. Based on the calculation of the distortion parameters and the electric dipole moment of the $ClMn_6$ octahedron, it is considered theoretically and experimentally that the $ClMn_6$ octahedron is the structural unit that affects the pyroelectric properties of the boracite. Comparing $Mn_3B_7O_{13}Cl$ and $Ni_3B_7O_{13}Cl$, the results show that the M-site metal atoms will affect the distortion degree of polyhedron, and then affect the polarization of the sample, and finally affect the pyroelectric property. The infrared spectrum analysis further confirms this conclusion.The above finding may provide some useful insights for the further study on the pyreolectricity of boracite.

Declarations

CRediT authorship contribution statement

Qiangqiang Wang: Formal analysis, Investigation, Writing – original draft. Jiesen Guo: Formal analysis, Investigation. Ruijin Sun: Conceptualization, Methodology, Writing – original draft. Yuetong Wu: Writing – review & editing. Yuxin Ma: Investigation. Fei Chen: Validation. Tianming Liu: Writing – review & editing. Haodong Li: Writing – review &editing.Fanshu Meng: Writing – review &editing Dezhong Meng: Writing – review & editing. Changchun Zhao: Conceptualization.

Declaration of Competing Interest

The authors declare that they have no known competing financial interests or personal relationships that could have appeared to influence the work reported in this paper.

Acknowledgements

We gratefully acknowledge the financial support from the State National Natural Science Foundation of China. (Grant Nos.51472224, 52102338) 2022 Discipline Development Research Foundation of China University of Geosciences, Beijing (640200009).

References

1. Honea R M B, Frank R (1962) Chambersite, a new mineral. American Mineralogist 47: 665-671.
2. Kubel F, Crottaz O J Z F K (1996) Crystal structure of manganese chlorine boracite, Mn3B7O13Cl. Zeitschrift für Kristallographie - Crystalline Materials 211: 924. https://doi.org/10.1524/zkri.1996.211.12.924.
3. Castellanos-guzman G A, Burfoot J C, Schmid H, Tissot P (1981) Dielectric properties of orthorhombic Mn3B7O13Cl, Mn3B7O13Br, Mn3B7O13I boracites. Ferroelectrics 36: 411-414. https://doi.org/10.1080/00150198108218141.
4. Castellanos-Guzman A G In *200 years of research on boracites*, Proceedings of 1994 IEEE International Symposium on Applications of Ferroelectrics, 7-10 Aug. 1994; 1994; pp 6-9.
5. Crottaz O, Rivera J-P, Schmid H (1998) Piezoelectric effect and ferroelectric properties in Mn3B7O13I boracite. Journal of the Korean Physical Society 32: 1261-1264. https://archive-ouverte.unige.ch/unige:31135.
6. Xiong Z, He J, Hu B, Shan P, Wang Z, Su R, He C, Yang X, Long X (2020) Zn3B7O13Cl: A New Deep-Ultraviolet Transparency Nonlinear Optical Crystal with Boracite Structure. ACS applied materials & interfaces 12: 42942-42948. https://doi.org/10.1021/acsami.0c11162.
7. Wang Z, Qiao H, Su R, Hu B, Yang X, He C, Long X (2018) Mg3B7O13Cl: A New Quasi-Phase Matching Crystal in the Deep-Ultraviolet Region. Advanced Functional Materials 28: 1804089. https://doi.org/10.1002/adfm.201804089.
8. Xiong S, Liang D, Cao L, Sun J (2016) Microstructure and Luminescence characteristics of self-doped nano-Mn3B7O13Cl crystal. Materials Letters 178: 87-90. https://doi.org/10.1016/j.matlet.2016.04.196.
9. Schnelle W, Schmid H (2015) Magnetic and structural phase transitions of multiferroic boracitesM3B7O13X(M=3dtransition metal Cr–Zn or Mg;X=halogen Cl, Br, I). Physical Review B 91: 1-25. https://doi.org/10.1103/PhysRevB.91.184411.
10. Aihua L, Liqiang X, Shouli L, Yanyan H, Ranran Z, Yanjun Z (2015) One-dimensional manganese borate hydroxide nanorods and the corresponding manganese oxyborate nanorods as promising

anodes for lithium ion batteries. Nano Research 8: 554-565. https://doi.org/10.1007/s12274-014-0669-7.

11. Schmid H, Genequand P, Pouilly G, Chan P (1980) Pyroelectricity of Fe-I and Cu-Cl boracite. Ferroelectrics 25: 539-542. 10.1080/00150198008207065.
12. Campa-Molina J, Castellanos-Guzmán A G, Bárcena-Soto M, Reyes-Gómez J (1994) Pyroelectric, ferroelectric, dielectric and thermal properties of Mn3B7O13Br single crystals. Solid State Communications 89: 963-969. https://doi.org/10.1016/0038-1098(94)90361-1.
13. Bhalla A S, Cross L E, Newnham R E J J J o A P (1985) Glass Bonded Crystalline Boracite Composites for Pyroelectric Applications. 24: 454. https://doi.org/10.7567/JJAPS.24S2.454.
14. Kuznetsov S A, Paulish A G, Navarro-Cía M, Arzhannikov A V (2016) Selective Pyroelectric Detection of Millimetre Waves Using Ultra-Thin Metasurface Absorbers. Scientific Reports 6: 21079. https://doi.org/10.1038/srep21079.
15. Lheritier P, Torelló A, Usui T, Nouchokgwe Y, Aravindhan A, Li J, Prah U, Kovacova V, Bouton O, Hirose S, Defay E (2022) Large harvested energy with non-linear pyroelectric modules. Nature 609: 718-721. https://doi.org/10.1038/s41586-022-05069-2.
16. Zhang D, Wu H, Bowen C R, Yang Y (2021) Recent Advances in Pyroelectric Materials and Applications. Small (Weinheim an der Bergstrasse, Germany) 17: 2103960. https://doi.org/10.1002/smll.202103960.
17. Pandya S, Velarde G, Zhang L, Wilbur J D, Smith A, Hanrahan B, Dames C, Martin L W (2019) New approach to waste-heat energy harvesting: pyroelectric energy conversion. NPG Asia Materials 11: 26. https://doi.org/10.1038/s41427-019-0125-y.
18. Shirokov V B, Razumnaya A G, Yuzyuk Y I (2017) Tunable pyroelectric properties of barium strontium titanate thin films. Journal of Physics Condensed Matter 29: https://doi.org/10.1088/1361-648X/aa5711.
19. Jayalakshmy M S P, J. (2014) Pyroelectric figures of merit and associated properties of LiTaO3/poly vinylidene difluoride nanocomposites for thermal/infrared sensing. Sens. Actuator A-Phys. 206: 121-126. https://doi.org/10.1016/j.sna.2013.12.004.
20. Liang Z, Li S, Liu Z, Jiang Y, Li W, Wang T, Wang J (2015) High responsivity of pyroelectric infrared detector based on ultra-thin (10 μm) LiTaO3. Journal of Materials Science: Materials in Electronics 26: 5400-5404. https://doi.org/10.1007/s10854-015-3088-y.
21. Bhatti H S, Hussain S T, Hussain S (2016) Synthesis and induced multiferroicity of perovskite PbTiO3; a review. Appl. Surf. Sci. 367: 291-306. https://doi.org/10.1016/j.apsusc.2016.01.164.
22. Xu T, Wang J, Shimada T, Kitamura T (2013) Direct approach for flexoelectricity from first-principles calculations: cases for SrTiO3 and BaTiO3. Journal of physics-condensed matter 25: https://doi.org/10.1088/0953-8984/25/41/415901.
23. Yang J, Wang R, Wang H, Li T, Pan S, Zhang B (1994) Pyroelectricity and temperature-dependent domain structure of azobenzene derivative polar Langmuir-Blodgett films. Thin Solid Films 243: 536-539. https://doi.org/10.1016/0040-6090(93)04072-Z.

24. Lang S (2005) Pyroelectricity: From Ancient Curiosity to Modern Imaging Tool. Physics Today - PHYS TODAY 58: 31-36. https://doi.org/10.1063/1.2062916.
25. Guo J, Sun R, Chen F, Hao M, Ma Y, Wang Q, Wu Y, Hou D, Zhang Z, Liu T, Li Z, Meng D, Zhao C (2022) Crystal growth and functional properties of rare mineral Mn3B7O13Cl. Journal of Crystal Growth 581: 126510. https://doi.org/10.1016/j.jcrysgro.2021.126510.
26. Delfino M L, G. M. Gentile, P. S. (1980) Preparation and mechanistic studies of halogen boracites. Inorganica Chimica Acta 43: 59-63. https://doi.org/10.1016/S0020-1693(00)90504-8.
27. Wang Q, Xu H, Gao S, Yang L, Wu D, Tian Z, Sun Y (2013) Synthesis of the rare mineral chambersite and its ore deposit geological significance. Earth Science Frontiers 20: 123-130.
28. Nelmes R J (1974) Structural studies of boracites. A review of the properties of boracites. Journal of Physics C: Solid State Physics 7: 3840-3854. https://doi.org/10.1088/0022-3719/7/21/008.
29. McQuaid R G P, Campbell M P, Whatmore R W, Kumar A, Gregg J M (2017) Injection and controlled motion of conducting domain walls in improper ferroelectric Cu-Cl boracite. Nature Communications 8: 15105. https://doi.org/10.1038/ncomms15105.
30. Sun Y, Li Z, Lee M-H, Yang Z, Pan S, Sadeh B (2017) First-Principles Assisted Prediction of the Nonlinear Optical Behavior of Mg3B7O13Cl Crystal. Journal of the Physical Society of Japan 86: 044401. https://doi.org/10.7566/JPSJ.86.044401.
31. Ju J L, Hongmei. Wang, Yingxia. Lin, Jianhua. Dong, Cheng (2002) A novel synthesis approach to transition metal boracites. Journal of Materials Chemistry 12: 1771-1774. https://doi.org/10.1039/B109461K.
32. Sri Gyan D, Sundram V, Dwivedi A, Bhowmick S, Maiti T (2020) Effect of B-site cation ordering on high temperature thermoelectric behavior of BaxSr2−xTiFeO6 double perovskites. Journal of Physics: Condensed Matter 32: 235401. https://doi.org/10.1088/1361-648X/ab7575.
33. Khatun A, Sk S, Pandey S K (2022) Understanding the Seebeck coefficient of LaNiO3 compound in the temperature range 300-620 K. Journal of physics-condensed matter 34: https://doi.org/10.1088/1361-648X/ac462a.
34. Zhou G, Liu H, Chen K, Gai X, Zhao C, Liao L, Shen K, Fan Z, Shan Y (2018) The origin of pyroelectricity in tourmaline at varying temperature. Journal of Alloys and Compounds 744: 328-336. https://doi.org/10.1016/j.jallcom.2018.02.064.
35. Chen K, Gai X, Zhou G, Shan Y, Zhao C, Shen K, Fan Z (2019) Study on a new type of pyroelectric materials with structure of tourmaline. Ceramics International 45: 10684-10690. https://doi.org/10.1016/j.ceramint.2019.02.139.
36. Jachalke S, Mehner E, Stocker H, Hanzig J, Sonntag M, Weigel T, Leisegang T, Meyer D C (2017) How to measure the pyroelectric coefficient? APPLIED PHYSICS REVIEWS 4: https://doi.org/10.1063/1.4983118.
37. Meirzadeh E, Christensen D V, Makagon E, Cohen H, Rosenhek-Goldian I, Morales E H, Bhowmik A, Lastra J M G, Rappe A M, Ehre D, Lahav M, Pryds N H, Lubomirsky I J A M (2019) Surface Pyroelectricity in Cubic SrTiO3. Adv. Mater. 31: https://doi.org/10.1002/adma.201904733.

38. Chang H Y, Kim S H, Halasyamani P S, Ok K M (2009) Alignment of lone pairs in a new polar material: synthesis, characterization, and functional properties of Li2Ti(IO3)6. J. Am. Chem. Soc. 131: 2426-2427. https://doi.org/10.1021/ja808469a.
39. Ertl A, Hughes J M, Pertlik F, Foit F F, Wright S E, Brandstatter F, Marler B J C M (2002) Polyhedron distortions in tourmaline. The Canadian Mineralogist 40: 153-162. https://doi.org/10.2113/gscanmin.40.1.153.
40. Song Z, Liu Q (2019) Effect of polyhedron deformation on the 5d energy level of Ce3+ in lanthanide aluminum perovskites. Physical Chemistry Chemical Physics 21: 2372-2377. https://doi.org/10.1039/C8CP06052E.
41. Zhang L (1993) Bond-valence sum and distortion of coordination polyhedra. Chinese Journal of Geochemistry 12: 92-96. https://doi.org/10.1007/BF02869049.

Figures

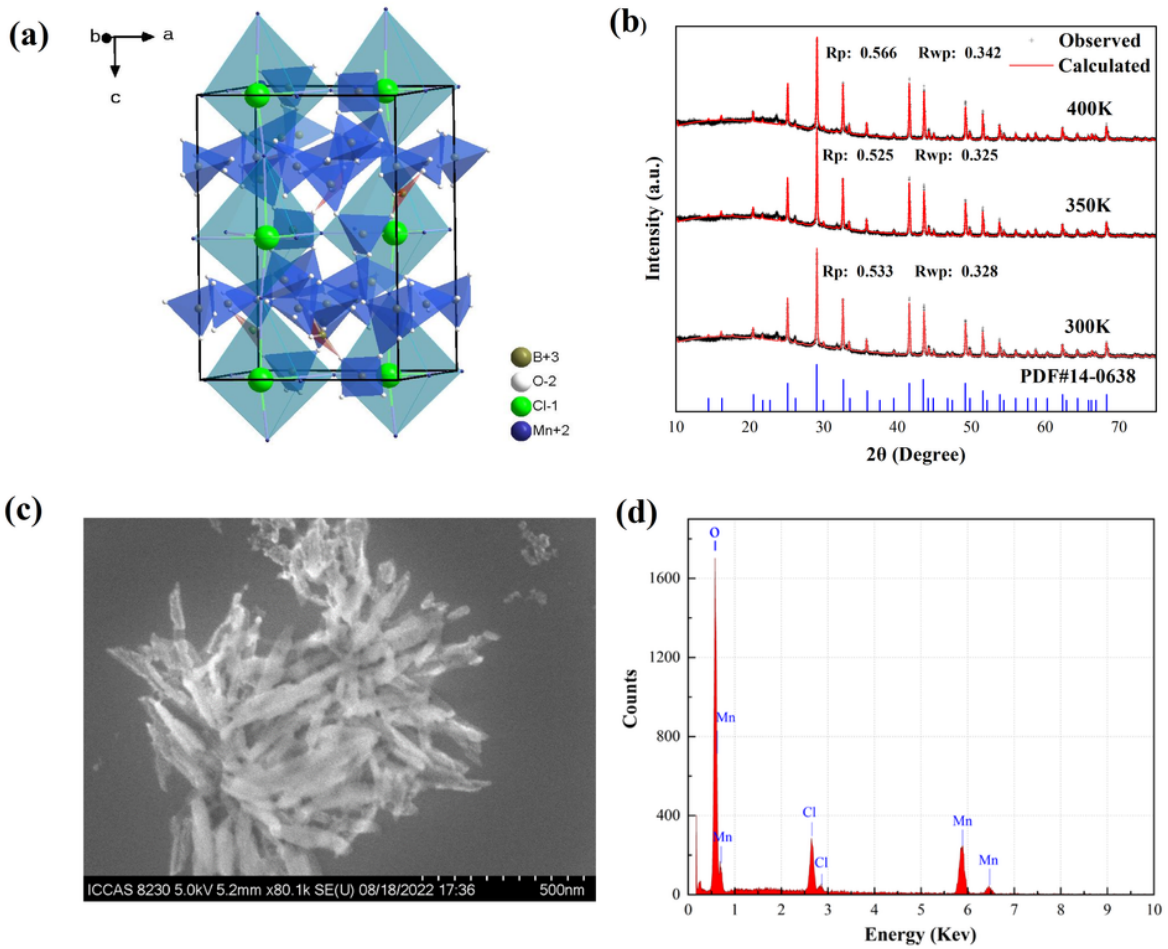

Figure 1

(a) Crystal structure of $Mn_3B_7O_{13}Cl$. (b) Observed (+) and calculated (line) profiles of X-ray powder patterns of $Mn_3B_7O_{13}Cl$ as a result of the Rietveld analysis at different temperatures (PDF#14-0638) (PDF#14-0638). The SEM images (c) and EDS spectrum (d) of the $Mn_3B_7O_{13}Cl$.

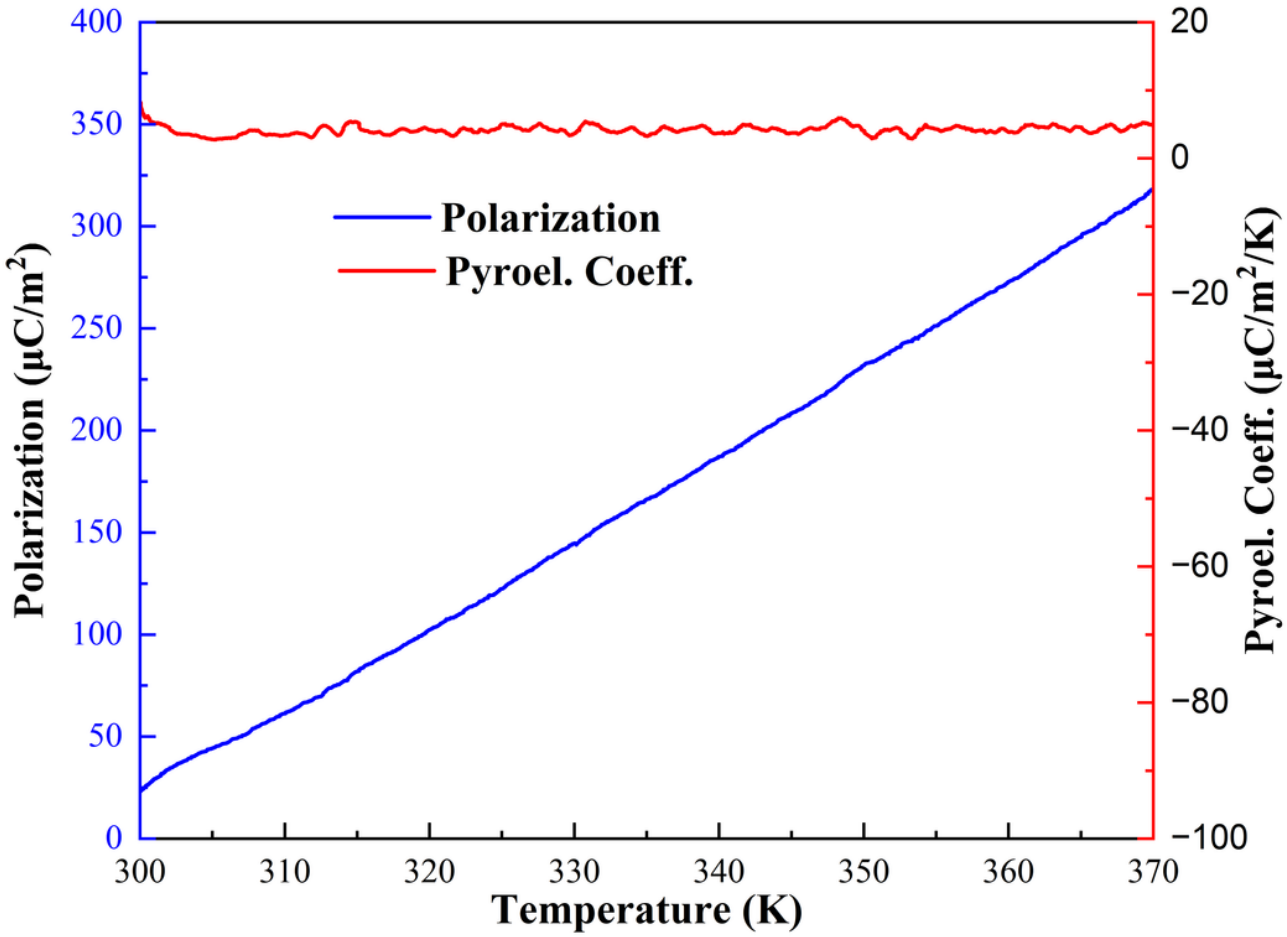

Figure 2

The Pyroelectric Coefficient and Change of Polarization intensity(|ΔP|)

of $Mn_3B_7O_{13}Cl$.

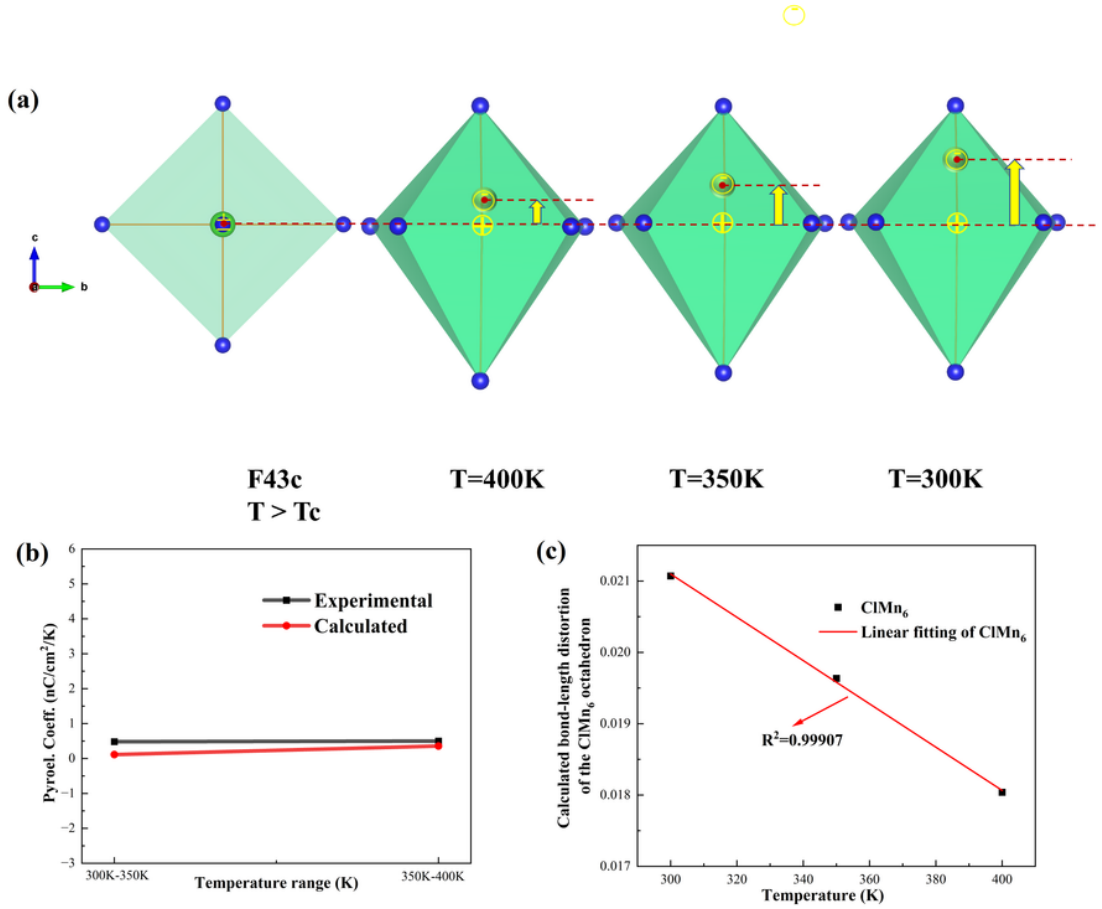

Figure 3

(a) Schematic diagram of the electric dipole as a function of temperature. (b) Comparison of calculated and experimental pyroelectric coefficients of $Mn_3B_7O_{13}Cl$. (c) Calculated bond-length distortion of the ClMn6 octahedron at different temperature.

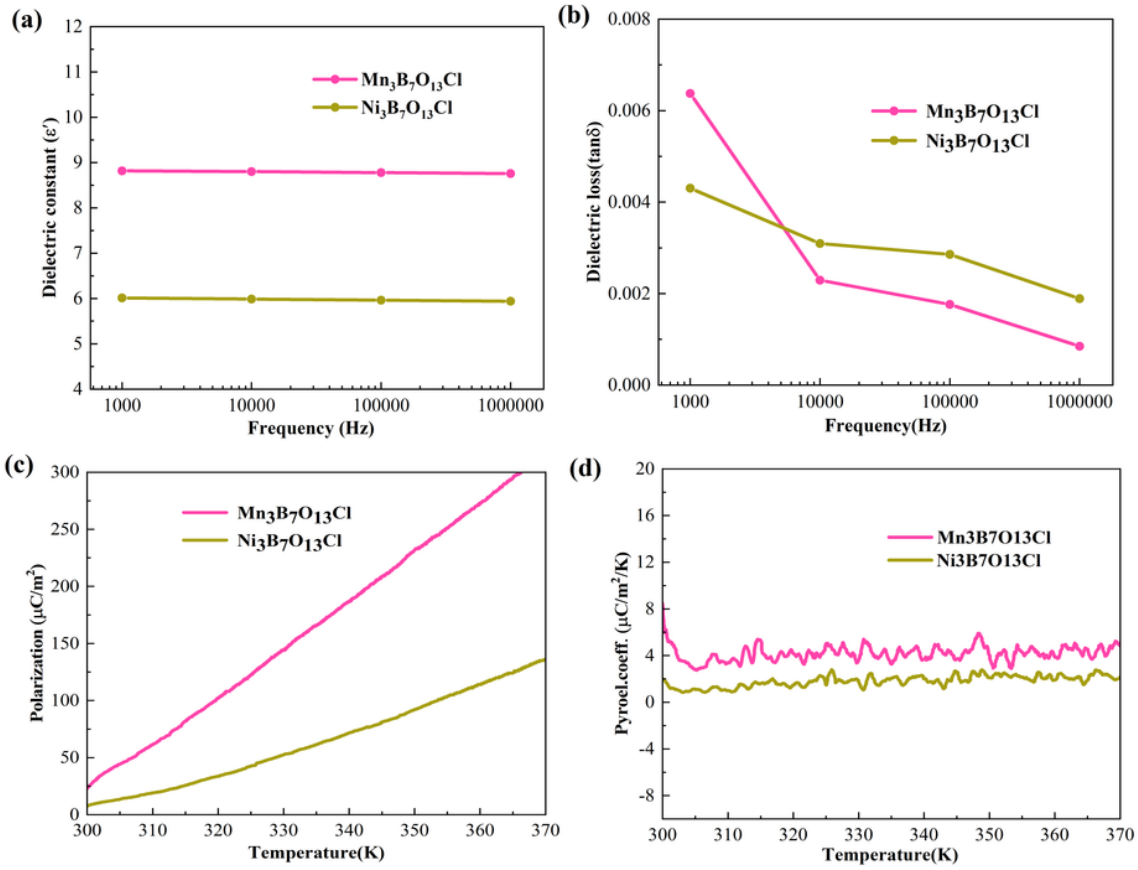

Figure 4

The measurement results of dielectric constant(a), dielectric loss(b), spontaneous polarization(c) and pyroelectric coefficient(d) of $Mn_3B_7O_{13}Cl$ and $Ni_3B_7O_{13}Cl$.

Supplementary Files

This is a list of supplementary files associated with this preprint. Click to download.

- Supplementarymaterialanddata.docx